PAPER 76 – IMPACT OF SUPPORT GEOMETRY ON THE PUNCHING SHEAR BEHAVIOR OF REINFORCED CONCRETE FLAT SLABS

M. A. Akinpelu[1], D. S. Gabriel[1], A. M. Salman[1]

[1]Department of Civil Engineering, Kwara State University, Malete, Kwara State, Nigeria. (10 points)
*Email: mutiu.akinpelu@kwasu.edu.ng

ABSTRACT
This study was carried out to assess the impact of support geometry on the punching behaviour of flat slabs using Abaqus Finite Element modelling software. The support geometrical constraint considered herein is strictly the column shapes. The first numerical specimen was developed using specifications of a previously tested experimental model and the simulation accuracy was validated by comparisons to experimental results. Three other variants of the validated model were developed by replacing the square column support with different shapes of column supports. The support shapes considered are L, T and Cruciform. The finite element analysis study showed that the influence of column geometry becomes visible only after the first initial crack had been developed in the slab. Although all simulated slabs indicated similar failure modes in the form of a sudden collapse at peak load signifying a typical shear failure. In conclusion, it was noted that the Cruciform shaped support column provided the highest shear resistance with a magnitude of 582.8 kN while 475 kN, 493.9 kN, and 502 kN were recorded in Square, L, and T-shaped support respectively.

KEYWORDS: Punching shear, Flat Slab, Column Shape, Finite Element.

1.0 INTRODUCTION

Flat slabs are primarily slabs that are without beams or any intermediate structural elements aiding in transferring loads to the columns. Hence, they have a direct transmission of loads and connection with columns. This system of flooring is becoming most adopted in various structures ranging from medium-rise to high risers and also in facilities such as garages, factories, airports, hospitals, multi-purpose buildings and skyscrapers. Their use is much more prevalent in skyscrapers and high risers which are sensitive to heights and the number of floors. As the number of floors increases, there is an inevitable need for machine floors which in turn reduces the number of available spaces. Therefore, a smaller headroom is readily adopted not only to reduce heights and increase the number of floors but also to ensure minimal barriers to the mechanical, electrical and all other servicing fittings.

On the other hand, one of the major structural sets for these types of slab is its inherent ability to fail in punching shear. Punching shear is caused by the concentration of loads from the supporting columns transferred to the slab in form of stress. This failure occurs as the slab gives way for the vertical bulging of the column through the slab in form of shear. Punching occurs both in axisymmetric and unsymmetric slabs. In the later cases, the stresses occur due to concentrated forces and moments induced by the eccentricity of reactions, while in the formal scenario failure and deformations are experienced mainly from the effects of concentrated force causing a trumpet or conical-shaped inclined cracks propagating through the slab around the perimeter of the column or wall at an angle between 20^o-30^o. (CEB-FIP, 1991).

However, over the decades punching shear behaviour has been an active field of interest and it has been investigated by various researchers. Varieties modelling methodology has been developed over time to simulate the behaviour of punching shear in slabs. Also, a series of databases has been initiated over the years to give a reference to the series of experimental tests carried out by different researchers. Whereas, they as much as possible try to postulate substantial possible scenarios, the research has been confined and some of the derived models are yet to be understood (Perez & Jalal, 2020).

The exact solution to most hands-on problems in engineering is very complex and the punching shear phenomenon is not exempted. The analytical approaches often involved the formation of mathematical models of the variables affecting the problem solution such as stresses and strain distribution in a solid structure. It is a common phenomenon in such procedures to replace the complex system with a simplified model that could be easily solved by an analytical approach (Akinpelu & Adedeji, 2018). Simplified models often come with many assumptions and uncertainties. Because of these, large "factors of safety" were introduced to ensure the safety of structures designed by this procedure. This is one of the reasons analytical results are highly conservative when compared to experimental results. However, with the advent of high-speed computers, the recent trend in the analysis of engineering problems embraced the use of more versatile numerical techniques. One of the most widely used numerical methods is Finite Element Method (FEM). To this end, in attaining the aim of this research, Abaqus finite element software 2021 was used to conduct all numerical analysis simulations.

2.0 THEORETICAL ANALYSIS

2.1 Abaqus Finite Element Methods

The governing equilibrium equation of discretized FE model derived from the principle of virtual work can be written symbolically in terms of displacement (*u)* as expressed in Equation 1:

$$F^N(u^M) = 0 \qquad \text{(Eqn 1)}$$

where F^N is the force component conjugate to the N^{th} variable and is the value of M^{th} variable displacement.

Due to the nonlinear stress-strain relationship of most engineering problems, the governing equation, Equation 1, emanated from the nonlinear equation of strains and thus, the function is nonlinear. Numerical methods are therefore required to solve the equation for a given set of forces. Besides, since the result of the governing equation is history-dependent, the solution must be sourced through incremental analysis of the external forces in order to capture the displacements, strains and stresses of time history along with the applied forces. Abaqus software basically utilises Newton-Raphson numerical procedure to solve the nonlinear equilibrium equation. The method is preferred to alternate procedures due to its high convergence rate.

2.2 Material Constitutive Model

2.2.1 Concrete Material

Numerous studies have supported the use of the Concrete Damage Plasticity Model (CPDM), which has been found to produce the most accurate results when compared to the experimental results and observations of reinforced concrete structure failure and post-failure (M. Akinpelu et al., 2021; Hafezolghorani et al., 2017; le Minh et al., 2021). The theory advanced by Lubliner et al., (1989) was applied to create the yielding criterion for this form model, along with modifications suggested by (Lee & Fenves, 1998) more details are found in (Dassault Systèmes, 2021). Three distinct stages of the concrete's plasticity, compressive behaviour, and tensile behaviour are taken into account during the calibration of CPDM. The sections below that follow discuss the theories and governing equations that were taken into consideration.

I) Concrete in Compression

The compressive stress characteristic data were generated using the (Eurocode 2, 2004) model for non-linear structural analysis.

The compressive stress and shortening strain for short-term uniaxial loading relationship was adopted from Equation 2 as defined in (Eurocode 2, 2004)

$$\frac{\sigma_c}{f_{cm}} = \frac{k\eta - \eta^2}{1+(k-2)\eta} \qquad \text{(Eqn. 2)}$$

The denotations in Eqn. 2 are as defined in Eqn. 3-8

$$\eta = \frac{\varepsilon_c}{\varepsilon_{c1}} \qquad \text{(Eqn. 3)}$$

$$\varepsilon_u = 0.0035 \ (f_c < 50 \ \mathrm{N/mm^2}) \quad \text{(Eqn. 4)}$$

$$\varepsilon_{c1} = \left(\frac{0.7 f_{cm}^{0.31}}{100}\right) < 2.8 \quad \text{(Eqn. 5)}$$

$$\varepsilon_{cu} = (2.8 + 27[(98 - f_c)/100]^4) \quad (f_c < 50 \ N/mm^2) \quad \text{(Eqn. 6)}$$

$$k = 1.1 E_C \times \left(\frac{\varepsilon_u}{f_{cm}}\right) \quad \text{(Eqn. 7)}$$

$$f_{cm} = f_c + 8 \quad \text{(Eqn. 8)}$$

Where:
fc is the characteristic cylindrical compressive strength of concrete at 28 days.
$f$cm is the mean value of concrete cylinder compressive strength.
Ɛc is the strain at peak stress
Ɛc1 is the ultimate strain

II) Concrete in Tension

The following (Equation 9-10) describes analytical models are as defined suitable by (Cornelissen et al., 1986), with terms and symbols modifications from (Genikomsou & Polak, 2016)

$$\frac{\sigma}{f_t} = \left(\left(1 + \left(\frac{c_1}{w_c}\right)^3\right) e^{-\left(\frac{c_2 w}{w_c}\right)}\right) - \left(\left(\frac{w}{w_c}\right)(1 + c_1^3) e^{-c_2}\right) \quad \text{(Eqn. 9)}$$

$$w_c = 5.14 \left(\frac{G_f}{f_t}\right) \quad \text{(Eqn. 10)}$$

Where; c_1 and c_2 are materials coefficients determined to be 3 and 6.93 respectively and w_c is the critical crack opening width, f_t is the tensile strength of concrete. While G_F is as established in (CEB-FIP, 1991) denoting the energy needed to propagate a tensile crack of a unit area given as;

$$G_F = G_{F0}(f_{cm}/f_{cmo})^{0.7} \quad \text{(Eqn. 11)}$$

f_{cmo} is taken as 10, and G_{F0} is expressed as a coefficient which is dependent on the maximum aggregate size. Hence the derived value of 0.065 J/m^2 were adopted as G_f assuming a maximum aggregate size d_{max} of 16mm

2.3 Steel Material

Steel Reinforcement Constitutive Model

The constitutive behaviour of steel material is identical in tension and compression. For this study, the stress-strain behaviour of reinforcing steel was modelled as a linear elastic, linear strain hardening material. The two elastic constants defined the linear elastic isotropic properties of the steel material while the plastic strains (obtained as total strains minus the elastic strains) and the yield strengths as presented in Table 1 defined the plastic property of the material adopted.

3.0 METHODOLOGY

3.1 Description of the Experimental Model

A flat slab specimen tagged RS, out of a series of test specimens experimented for punching at the University of Brasilia and reported by (Lima, 2021; R. de A. Palhares, 2018), was adopted. The tested specimen details is as presented in Fig. 2a and 2b. The slabs were loaded to failure by gradual increment through hydraulic jacks at 8 distinct points having radial dimensions of 1124 mm from the centre of the column as shown in Figure 3. The resulting mechanical properties of the materials are recorded in the adopted literature and presented in Table 1 and Table 2.

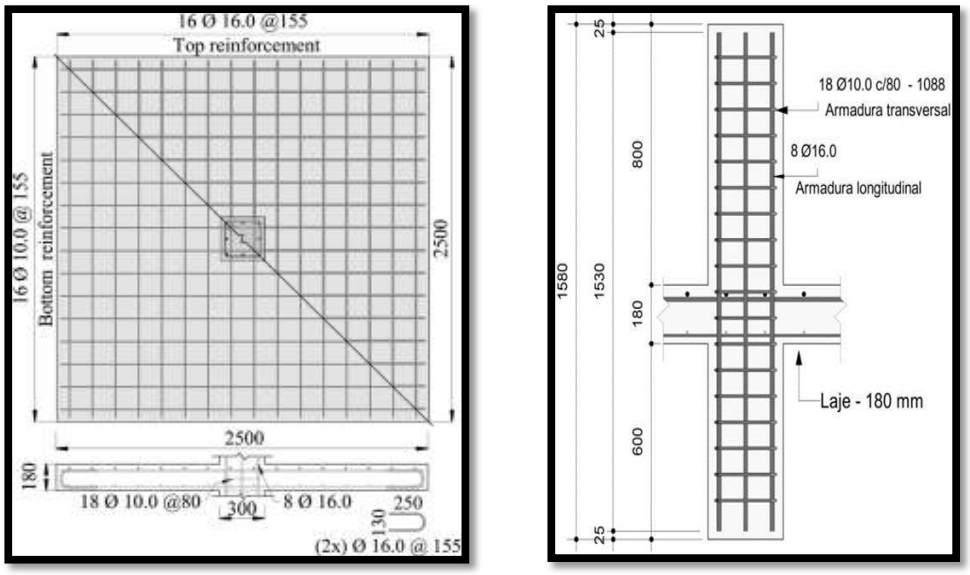

a) Slab reinforcement details b) Column reinforcement details

Fig. 1: Reinforcement arrangements in slab RS (all dimensions in mm)
(Lima, 2021; R. A. Palhares et al., 2022)

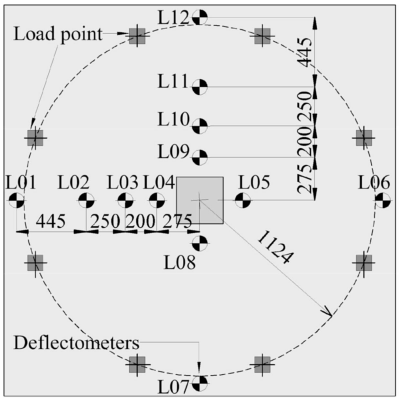

Fig. 2: Loading and deflectometer arrangements as used in the test system (all dimensions mm)
(Lima, 2021; R. A. Palhares et al., 2022)

Table 1: Mechanical Properties for the Reinforcement Steel

Bar diameter (mm)	Ultimate Yied stress (f_y) (N/mm^2)	Modulus of Elasticity (E_s) (N/mm^2)
16	549	196900
10	515	126600

(Source: (R. de A. Palhares, 2018)

Table 2: Mechanical Properties for the Concrete material

Slab	mean compressive strength, f_c (N/mm^2)	Average tensile strength*, f_{tm} (N/mm^2)	Modulus of Elasticity* (N/mm^2)
RS	29.9	2.89**	32,810*

(Source: (R. de A. Palhares, 2018)
*The average elastic modulus and tensile strength of concrete were calculated using Eurocode 2 (2004) as stated in Eqn 12 and 13 respectively.

$*E_C = 22\ [\ (f_c + 8)/10]^{0.3} * 10^3$ Eqn. 12

$**f_{tm} = 0.3 * f_c^{2/3}$ Eqn. 13

3.2 Description of Numerical models

The experimental model as defined in section 3.1 was used as a basis for the development and calibration of the control model (specimen with square support). The precision of the control model was validated by comparison with experimental results. The validated model was subsequently extended to develop other specimens by replacing the square support shape with L,T and cruciform consecutively. The calibrating parameters adopted in the numerical simulations are stated in Table 3. It is noteworthy that the columns were of the same surface area as that used in the experimental and control model even as the geometrical shape differs. The details of the substituting supporting columns are as shown in Fig. 3. Also, it was ensured that there was no moment inducing eccentricity via the support-slab connection, this implies that the slab was loading axially as the centroid of the slab was ascertained to coincide with that of the supporting column.

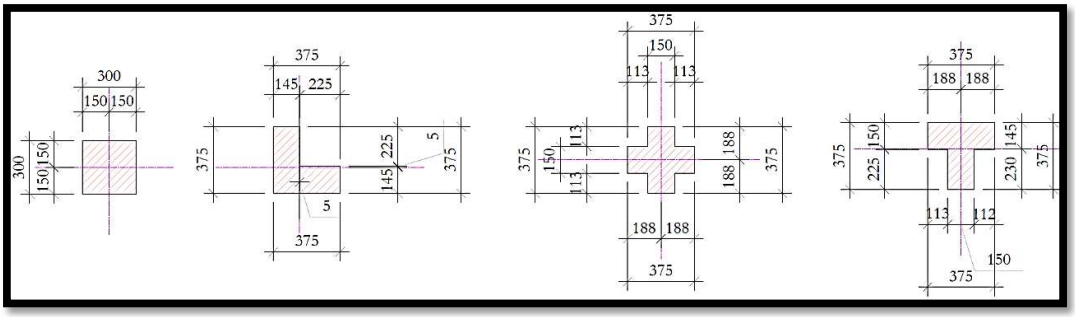

Fig. 3: Geometrical properties of different column shapes used in finite element simulations

Table 3: Material constitutive model parameters

Material	Parameter
Concrete	Model - CDPM Poisson ratio = 0.2 Young Modulus = 32,810 N/mm^2 (Eurocode 2, 2004) Dilation Angle, ψ = 25˚ (R. A. Palhares et al., 2022) Viscosity = 0.0001 (M. Akinpelu et al., 2021) Flow Potential Eccentricity = 0.1 (Default value) Stress ratio = 1.16 (Default Value) K = 0.667 (Default Value) Compressive stress-stress data = Eurocode 2, 2004 model Tensile stress-strain data = (Cornelissen et al., 1986) Element type =C3C8R Mesh Density 30x30mm (Wosatko et al., 2019)
Steel	Model – Linear elastic, linear strain hardening model Young modulus, Es = Experimental value (See table 1) Poisson ratio = 0.3 Element Type = T3D2

4.0 RESULT AND DISCUSSION

4.1 Model Validation

The load-displacement response graph (Figure 4) reveals that after the first crack was observed, the nonlinearity of the response to load is exhibited. However, there was continued resistance to the load effect but at a certain level of load exertion there is a sudden fall in the load resistance, this signifies the punching shear phenomenon. The aforementioned trend was similarly observed in the Finite element model and Experimental response signifying a good agreement between both models. Although there was a disparity in the initial stiffness behaviour, this has been attributed to microcracks development which could not be captured by the experimental instrumentation (M. A. Akinpelu & Adedeji, 2018).

The accuracy of the developed numerical model was further verified by comparison of the rupture surface deformation pattern in Fig. 5. Both models show correlating deformation pattern consistent with the conical shape formation as predicted by previous literature (R. A. Palhares et al., 2022).

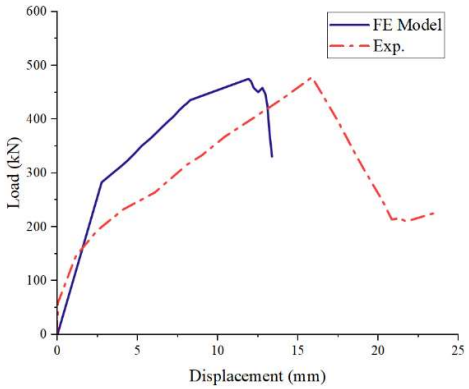

Figure 4: FEM versus experimental load-deflection response for the flat slabs

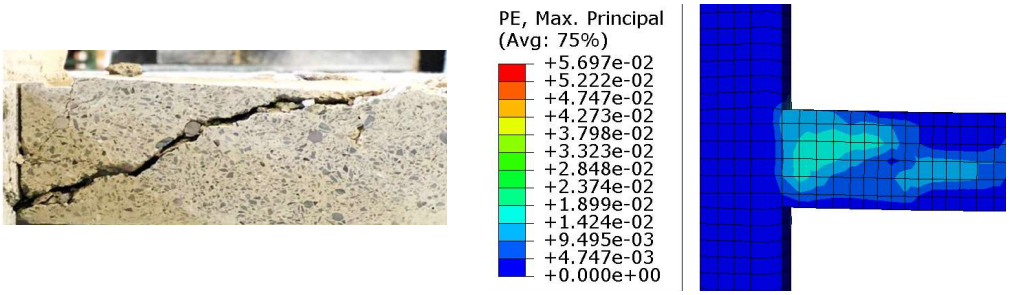

Figure 5: Experimental versus FEM rupture surface at failure.

4.2 Effect of Support Geometry of Punching shear behaviour of flat slabs

The load displacement response of the various considered model is as comparatively presented in Fig. 6. It can be observed that at the initial stages of loading where the structure is fully elastic and deformation is yet commence, the effect of variating column support shapes are negligible. However, after the initial stage where the response tends show nonlinearity given the development of tangential cracks within the model. It was observed that the stiffness response of various model differs and the magnitude of peak load resistance (Punching shear capacity) varies across the models considered (see Figure 7). Nevertheless, as discussed in Section 4.1 the failure mode (punching shear) of the various specimens is revealed to be insensitive to changing of the column shapes.

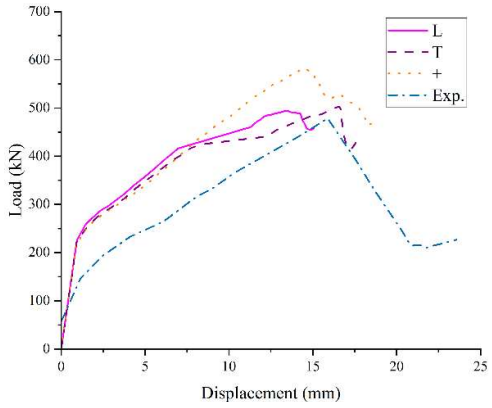

Figure 6 : Comparative graph showing the load-displacement response of various flat slab specimens

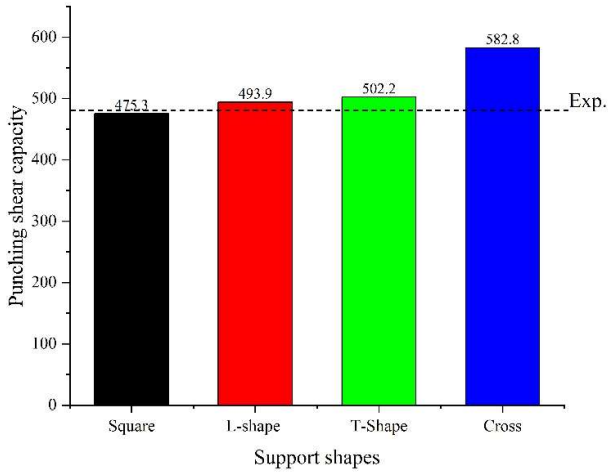

Figure 7: Comparative graph showing Punching shear capacity of various flat slab specimens

5.0 Conclusions

1. The developed finite element model precisely imitates the load-displacement behaviour of reinforced concrete flat slabs.
2. According to the results of the finite element analysis study, the influence of column geometry is only apparent after the slab has already developed its first crack. Despite that, all simulated slabs showed a similar failure mode in the form of a sudden, continuous drop in load resistance at a certain stage of load exertion representing a typical shear failure.
3. The finite element results reveal that the geometrical shape of the supporting column substantially influences the punching shear resistance of flat slabs. Deductively, cruciform shaped support column provided the highest shear resistance with a magnitude of 582.8 kN while 475 kN, 493.9 kN, and 502 kN were recorded in Square, L, and T-shaped support respectively.

References

Abaqus - SIMULIA User Assistance 2021. Retrieved February 14, 2023, from https://help.3ds.com/2021/english/dssimulia_established/SIMULIA_Established_FrontmatterMap/sim-r-DSDocAbaqus.htm?contextscope=all&id=b15ba98a76ce4305b417ecdd54e5394d

Akinpelu, M. A., & Adedeji, A. A. (2018). Structural Response of Reinforced Self-Compacting Concrete Deep Beam Using Finite Element Method. *Journal of Soft Computing in Civil Engineering*, *2*(1), 36–61. https://doi.org/10.22115/SCCE.2018.50115

Akinpelu, M., Ibitoye, B., Samson O., O., & Olorede, K. (2021). Numerical Verification of Strut and Tie Models and Failure Modes of Reinforced Self-Compacting Concrete Deep Beams. *International Journal of Engineering Research in Africa*, *53*, 76–100.

British Standards Institution, & European Committee for Standardization. *Eurocode 2 : design of concrete structures - part 1-1 :general rules and rules for buildings.* 226. Retrieved January 21, 2023, from https://www.en-standard.eu/bs-en-1992-1-1-2004-a1-2014-eurocode-2-design-of-concrete-structures-general-rules-and-rules-for-buildings/

CEB-FIP, C. (1991). Model Code 1990. *Comite Euro-International Du Beton, Paris*, 87–109.

Cornelissen, H. A. W., Hordijk, D. A., & Reinhardt Summary, H. W. (1986). Experimental determination of crack softening characteristics of normalweight and lightweight concrete.

HERON, 31 (2), 1986. https://repository.tudelft.nl/islandora/object/uuid%3A08c29b39-5c60-4ab6-b9d5-643d11007f7c

Genikomsou, A., & Polak, M. A. (2016). *Damaged plasticity modelling of concrete in finite element analysis of reinforced concrete slabs*. https://doi.org/10.21012/FC9.006

Hafezolghorani, M., Hejazi, F., Vaghei, R., Jaafar, M. S. bin, & Karimzade, K. (2017). Simplified damage plasticity model for concrete. *Structural Engineering International*, *27*(1), 68–78. https://doi.org/10.2749/101686616X1081

Institution, B. S., & Standardization, E. C. for. (2004). *Eurocode 2: Design of Concrete Structures : Part 1-1: General Rules and Rules for Buildings*. British Standards Institution. https://books.google.com.ng/books?id=DIw3AgAACAAJ

le Minh, H., Khatir, S., Abdel Wahab, M., & Cuong-Le, T. (2021). A concrete damage plasticity model for predicting the effects of compressive high-strength concrete under static and dynamic loads. *Journal of Building Engineering*, *44*, 103239. https://doi.org/10.1016/J.JOBE.2021.103239

Lee, J., & Fenves, G. L. (1998). Plastic-Damage Model for Cyclic Loading of Concrete Structures. *Journal of Engineering Mechanics*, *124*(8), 892–900. https://doi.org/10.1061/(ASCE)0733-9399(1998)124:8(892)

Lima, H. J. N. de. (2021). *Análise experimental da resistência a punção em lajes lisas com armadura de cisalhamento parcialmente ancorada*. https://repositorio.unb.br/handle/10482/41379

Lubliner, J., Oliver, J., Oller, S., & Oñate, E. (1989). A plastic-damage model for concrete. *International Journal of Solids and Structures*, *25*(3), 299–326. https://doi.org/10.1016/0020-7683(89)90050-4

Palhares, R. A., Rossignoli, F. W., Sales de Melo, G., & Lima, H. (2022). A numerical model capable of accurately simulating the punching shear behavior of a reinforced concrete slab. *Structural Concrete*, *23*(2), 1134–1150. https://doi.org/10.1002/SUCO.202100773

Palhares, R. de A. (2018). *Análise experimental da punção em lajes lisas de concreto armado com variação da ancoragem da armadura de cisalhamento*. https://repositorio.unb.br/handle/10482/34298

Perez, J. A., & Jalal, P. (2020). *Punching Shear in Concrete Flat Slabs Supported on Slender Edge Steel Columns* [Concrete Structures]. KTH Royal Institute of Technology.

Wosatko, A., Winnicki, A., Polak, M. A., & Pamin, J. (2019). Role of dilatancy angle in plasticity-based models of concrete. *Archives of Civil and Mechanical Engineering*, *19*(4), 1268–1283. https://doi.org/10.1016/J.ACME.2019.07.003